inorganics

MDPI

Article

Enhancements in Hydrogen Storage Properties of Magnesium Hydride Supported by Carbon Fiber: Effect of C–H Interactions

Quan Yang [1], Xiansong Jia [1], Zhikang Qin [1], Xiaoli Ding [1,*] and Yongtao Li [1,2]

[1] Key Laboratory of Green Fabrication and Surface Technology of Advanced Metal Materials of Ministry of Education, School of Materials Science and Engineering, Anhui University of Technology, Maanshan 243002, China; yq20001214@163.com (Q.Y.); jiaxiansongyj@163.com (X.J.); ahut.zhikangqin@gmail.com (Z.Q.); toni-li@163.com (Y.L.)

[2] Key Laboratory of Efficient Conversion and Solid-State Storage of Hydrogen & Electricity of Anhui Province, Anhui University of Technology, Maanshan 243002, China

* Correspondence: dingxiaoli@ahut.edu.cn

Abstract: Carbon-based materials with excellent catalytic activity provide new ideas for the development of magnesium-based hydrogen storage. C-H bonding interactions may play a key role in performance improvement. In this work, we comprehensively compare the magnesium-carbon cloth composites (CC) prepared by method of dry ball milling and wet impregnation. The results were that the hydrogen release activation energy (E_a) of MgH_2@CC composites prepared by wet immersion method was 175.1 ± 19.5 $kJ \cdot mol^{-1}$, which was lower than that of pure MgH_2 ($E_a = 213.9 \pm 6.4$ $kJ \cdot mol^{-1}$), and the activation energy of MgH_2-CC composites prepared by ball milling method was 137.3 ± 8.7 $kJ \cdot mol^{-1}$, which provided better results. The kinetic enhancement should be attributed to C-H interactions. The presence of carbon carriers and electron transfer to reduce the activation energy of Mg-H bond fracture. These results will provide further insights into the promotion of hydrogen ab-/desorption from metal hydrides.

Keywords: hydrogen storage; magnesium-carbon composites; preparation methods; carbon-hydrogen bond

check for updates

Citation: Yang, Q.; Jia, X.; Qin, Z.; Ding, X.; Li, Y. Enhancements in Hydrogen Storage Properties of Magnesium Hydride Supported by Carbon Fiber: Effect of C–H Interactions. *Inorganics* **2024**, *12*, 273. https://doi.org/10.3390/inorganics12110273

Academic Editor: Maurizio Peruzzini

Received: 29 August 2024
Revised: 20 October 2024
Accepted: 22 October 2024
Published: 23 October 2024

1. Introduction

Energy is a potential driver of human production and social activity, and the depletion of fossil fuels and global climate change have prompted the search for clean energy carriers [1–3]. As a clean, efficient and abundant secondary energy source, hydrogen is considered one of the ideal energy carriers for storing and transferring energy in the future [4–8]. However, gaseous and liquid hydrogen storage have limitations in terms of safety and storage density for various applications [9–12]. Solid-state hydrogen storage, especially in the form of metal hydrides, offers the most compact and safe technology for storing hydrogen, and among the various solid-state hydrogen storage materials, MgH_2 is valuable for research due to its high hydrogen storage capacity (7.6%) and abundant magnesium metal resources (2.3%) [1,13–19]. However, the high thermodynamic stability and slow reaction kinetics of MgH_2 make it difficult to meet the requirements of practical applications [20–23].

Nanosizing [13,24–27] has been shown to be one of the effective ways to improve the thermodynamics/kinetics of the MgH_2 reaction, and chemical reduction and hydrogenation [28–31] have attracted interest due to their low cost and portable operating conditions [28,32]. Liu et al. [33] used carbon aerogel (CA) as a precursor, wet impregnated with dibutyl magnesium solution and hydrogenated to prepare Mg-CA composites. The average particle size of the Mg nanoparticles was 19.3 nm, and the enthalpies of hydrogenation and dehydrogenation were −65.1 and 68.8 $kJ \cdot mol^{-1}$. However, the hydrogen uptake kinetics of the Mg–CA composites were slower than those of the LaMg-containing ones prepared by the arc plasma method, and the kinetics need to be further improved.

In recent decades, a variety of novel carbon isomers have been synthesized, such as nanotubes [26,34], nanofibers [28,35], graphene [36,37], fullerenes [38,39], Mxenes [40,41], and carbon nanospheres [42,43]. Due to carbon's light weight, large specific surface area, thermal stability, load-bearing capacity, and carbon atom substitutability, the carbon composites studied those all contribute to enhance the kinetics of hydrogen uptake and/or desorption [44]. Carbon-based materials have been investigated as catalytic materials with the promise of further enhancing the MgH_2 kinetics. Andrey Lakhnik et al. [45] prepared MgH_2/C composites of elemental magnesium with graphite powder using high-energy ball milling method with particle sizes predominantly in the range of 10–30 μm. The materials have a minimum activation energy for hydrogen absorption of 65 $kJ \cdot mol^{-1}$ and a hydrogen capacity of ~4.3 wt%, which gives them an excellent kinetic performance. It was also found that the activation energy of the absorption process monotonically decreases with the increase of the graphite powder surface area during sample synthesis. Carbon composites also have excellent cycling performance, as they affect hydrogen storage kinetics primarily by preventing particle agglomeration and improving thermal conductivity [46]. R.M. Carson et al. [47] found that Mg-5 wt% C retains a capacity of 5.5 wt% H_2 after 1000 cycles and is suitable for most commercial applications.

The surface of carbon fiber has a high degree of surface defects and abundant growth sites, which can be used as a good growth carrier. Meanwhile, carbon fibers can improve cycling performance and inhibit MgH_2 agglomeration due to their hydrogen storage absorption/desorption cycling stability [8,48–50]. Herein, carbon fiber materials were selected to be combined with Mg-based hydrogen storage, and two different preparation processes, wet impregnation and dry ball milling, were designed in order to investigate the effect of the preparation processes on the hydrogen storage properties of magnesium-carbon fiber composites. It was found that the two preparation processes had a significant effect on the enhanced hydrogen storage kinetic properties of MgH_2. The introduction of carbon fiber carriers caused the carbon-hydrogen bond to weaken the interaction between hydrogen atoms and magnesium atoms, thus promoting the migration and release of hydrogen atoms.

2. Results and Discussion

2.1. Structural Features and Microstructures Induced by Different Processes

2.1.1. Structural Features of MgH_2@CC and MgH_2-CC Composites

We chose carbon fiber materials combined with magnesium-based hydrogen storage and designed two different preparation processes, wet impregnation and mechanical milling, as shown in Figure 1, with details as discussed in experimental sections. First, in order to investigate the formation process of MgH_2 on the carbon cloth, XRD tests were performed on the samples. The crystal structure analysis of MgH_2@CC and MgH_2-CC composites by XRD is shown in Figure 2a. The MgH_2@CC composite shows the presence of two broadened diffusion diffraction peaks near 25.2° and 43.1° that correspond to the characteristic diffraction peaks for carbon. The impregnated and vacuum-treated samples showed characteristic peaks of $MgBu_2$ near 12.4°, 19.2°, and 21.1°, respectively, indicating that the heptane solution had been completely removed and $MgBu_2$ was successfully loaded on the surface of the carbon cloth. The disappearance of the $MgBu_2$ phase and the appearance of the MgH_2 phase on the surface of the carbon cloth after the hydrogenolysis reaction imply that the hydrogenolysis reaction is complete. At the same time, no other heterogeneous phases appeared, suggesting that the dibutyl magnesium was completely transformed into MgH_2.

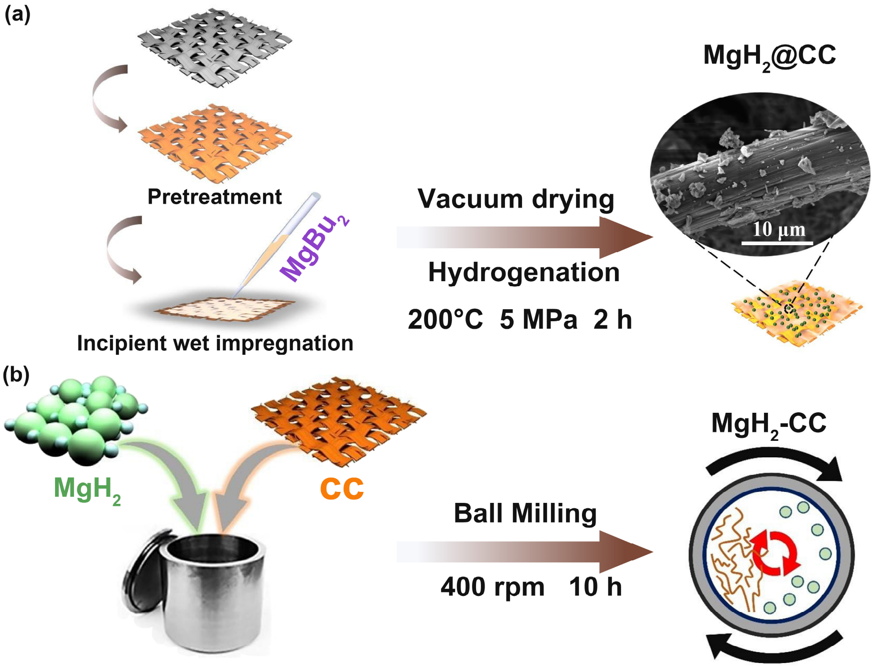

Figure 1. Schematic illustration of preparation process of (**a**) MgH_2@CC and (**b**) MgH_2-CC.

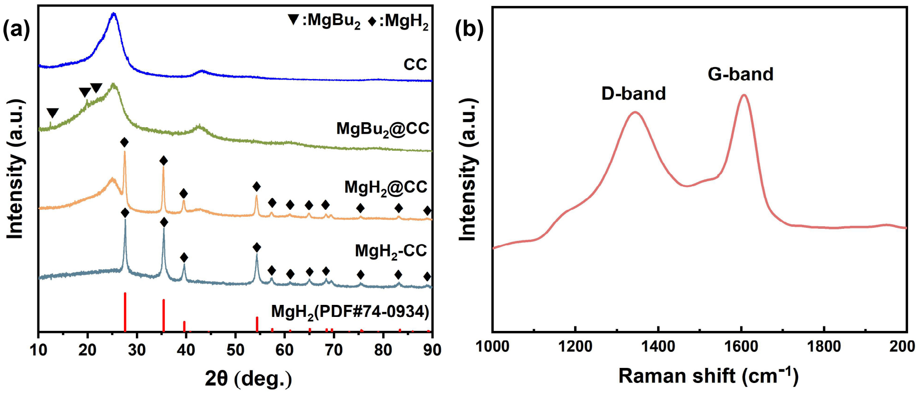

Figure 2. (**a**) XRD patterns of MgH_2@CC and MgH_2-CC composites and (**b**) Raman pattern of MgH_2-CC composites.

In addition, the MgH_2-CC composites prepared by ball milling showed characteristic peaks belonging to MgH_2 at 27.8°, 35.6°, and 39.7°, but no more obvious carbon peaks were detected, which may be attributed to the fact that the carbon fibers were uniformly dispersed in the MgH_2 matrix after ball milling. In order to demonstrate the successful loading of carbon fibers with MgH_2 in the MgH_2-CC composites, Raman tests were carried out on the MgH_2-CC composites. As shown in Figure 2b, typical Raman peaks belonging to the D-band and G-band of the graphite phase, respectively, appeared at wave numbers of 1350 cm^{-1} and 1590 cm^{-1}. D-band represents the sp3 defects in the carbon and the G-band represents the E2g vibration of the carbon due to the sp2 hybridization. The results also confirmed that the carbon fibers were successfully loaded with MgH_2 in the MgH_2-CC composites. The samples were then analyzed for particle size. The Scheller formula can be used to calculate the crystal size from the XRD data:

$$D = \frac{K\lambda}{\beta \cos\theta} \tag{1}$$

where D is the grain size perpendicular to the observed grain surface; K is a constant, usually taking the value of 0.9; λ is the wavelength of X-rays, β is the radian of the halfheight width of the sample's diffraction peak, and θ is the diffraction angle. According to the calculation results, the average grain size of MgH_2@CC is 35.75 nm, the average grain size of MgH_2-CC is 20.01 nm, and the average grain size of commercial MgH_2 is 181.56 nm, which are both improved.

2.1.2. Distinct Morphologies of MgH_2@CC and MgH_2-CC Composites

The microstructure of MgH_2@CC composites obtained by hydrogenolysis of organic magnesium was observed by scanning electron microscopy and is shown in Figure 3a–c. It can be clearly observed that the MgH_2 particles are uniformly distributed on the surface of the carbon fibers, and the high-density defects on the surface of the carbon cloth provide the growth sites for MgH_2, which grows along the direction of the rod-shaped carbon fibers. It was also observed that some of the MgH_2 on the surface of the carbon fibers was deposited due to physical changes during the impregnation process, but the MgH_2 particles on the surface still showed a diffuse distribution. The microstructure of MgH_2-CC composites obtained by ball milling is shown in Figure 3d–f. It can be clearly seen in the image that the MgH_2 particles and carbon fibers are diffusely distributed on the surface of the conductive adhesive, and the particles do not show an obvious aggregation phenomenon. Compared with MgH_2@CC composites, the particles are more uniformly dispersed, and it is easier to form a uniform carbon fiber loading system by the ball milling method, while the dispersed carbon after ball milling can inhibit the agglomeration of MgH_2 particles.

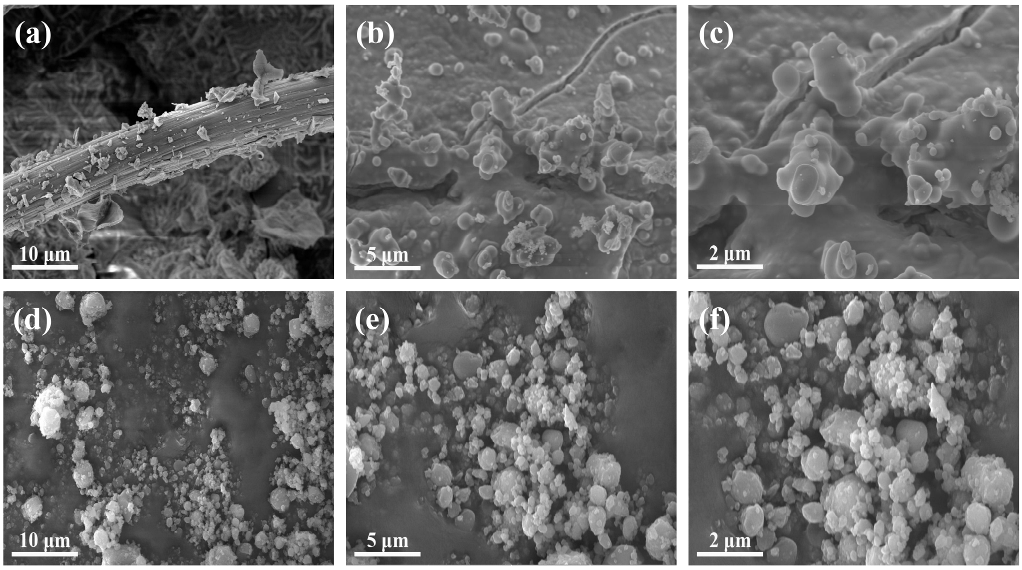

Figure 3. SEM images of (**a**–**c**) MgH_2@CC composites and (**d**–**f**) MgH_2-CC composites.

2.2. Improved Hydrogen Storage Performance

2.2.1. Kinetic Properties of MgH_2@CC and MgH_2-CC Composites

In order to investigate the kinetic properties of MgH_2@CC composites obtained after hydrolysis of organic magnesium, the composites were heated to 500 °C, with a heating rate of 3 °C/min, 5 °C/min, 8 °C/min, and 10 °C/min, and their DSC curves were tested. As a comparison, the DSC curves of commercially pure MgH_2 and BM-MgH_2 were tested under the same conditions. For the dehydrogenation, the exothermic decomposition of $MgH_2 \rightarrow Mg$ is accompanied by the exothermic process during the temperature rise stage, and the corresponding exothermic peaks will appear in the DSC curve. As shown in Figure 4, the peak exothermic temperatures of MgH_2-CC, MgH_2@CC, BM-MgH_2, and pure MgH_2 are 332 °C, 358 °C, 371 °C, and 449 °C, respectively. The peak hydrogen release temperatures of MgH_2-CC and MgH_2@CC composites were reduced by 117 °C and 91 °C, respectively, compared with that of pure MgH_2, indicating that the introduction of carbon fiber carriers can improve the kinetic properties of MgH_2 and reduce the peak hydrogen release temperature significantly.

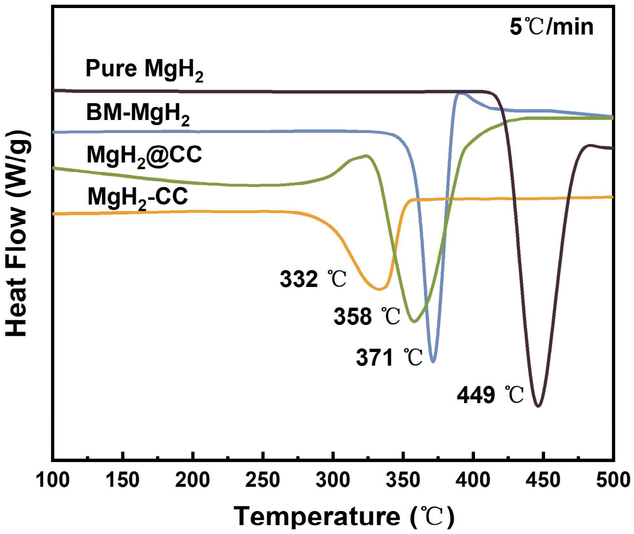

Figure 4. DSC curves of pure MgH_2, BM-MgH_2, MgH_2@CC and MgH_2-CC.

To further investigate the hydrogen release properties of MgH_2@CC and MgH_2-CC composites, Figure 5a–h shows the DSC curves of Pure MgH_2, BM-MgH_2, MgH_2@CC, and MgH_2-CC. It can be observed that both MgH_2@CC and MgH_2-CC show a significant decrease in the peak heat uptake temperature at different heating rates. The exothermic activation energy is also an important measure of the kinetic performance, and in general, the exothermic activation energy can be calculated based on the peak temperature of heat absorption and the rate of warming in combination with the Kissinger equation:

$$\ln\left(\frac{\beta}{T_P^2}\right) = \mathrm{A} - \frac{E_a}{\mathrm{R}T_P} \tag{2}$$

where β is the rate of temperature increase, T_p is the peak temperature of heat absorption, and A is a linear constant. The peak heat absorption temperatures of MgH_2@CC were 348.4 °C, 358.6 °C, 364.5 °C, and 372.1 °C at 3 °C/min, 5 °C/min, 8 °C/min, and 10 °C/min, respectively, and the scatter plots of $\ln(\beta/T_p{}^2)$ versus $1000/T_p$ were made subsequently, as shown in Figure 5b. Based on the slope of the straight line in the fitting result, the hydrogen release activation energy of MgH_2@CC can be obtained as ~175.1 $kJ\cdot mol^{-1}$, which is 38.8 $kJ\cdot mol^{-1}$ lower than that of commercially pure MgH_2 (213.9 $kJ\cdot mol^{-1}$), suggesting that the MgH_2@CC composites obtained by hydrolysis of organomagnesium improve their hydrogen release properties under the synergistic effect of nanoeffects and the carbon fiber carrier. Meanwhile, the hydrogen release properties of MgH_2-CC composites and BM-MgH_2 were investigated, and Figure 5e–h shows the DSC curves of MgH_2-CC composites and BM-MgH_2 and the straight line of $\ln(\beta/T_p{}^2)$ fitted to $1000/T_P$. It can be observed that the exothermic peak temperatures of MgH_2-CC composites are 321.3 °C, 332.8 °C, 341.5 °C, and 346.6 °C, respectively, and the activation energy of hydrogen release is ~137.3 $kJ\cdot mol^{-1}$, which is also significantly improved compared with that of the ball-milled MgH_2 samples (~176.4 $kJ\cdot mol^{-1}$).

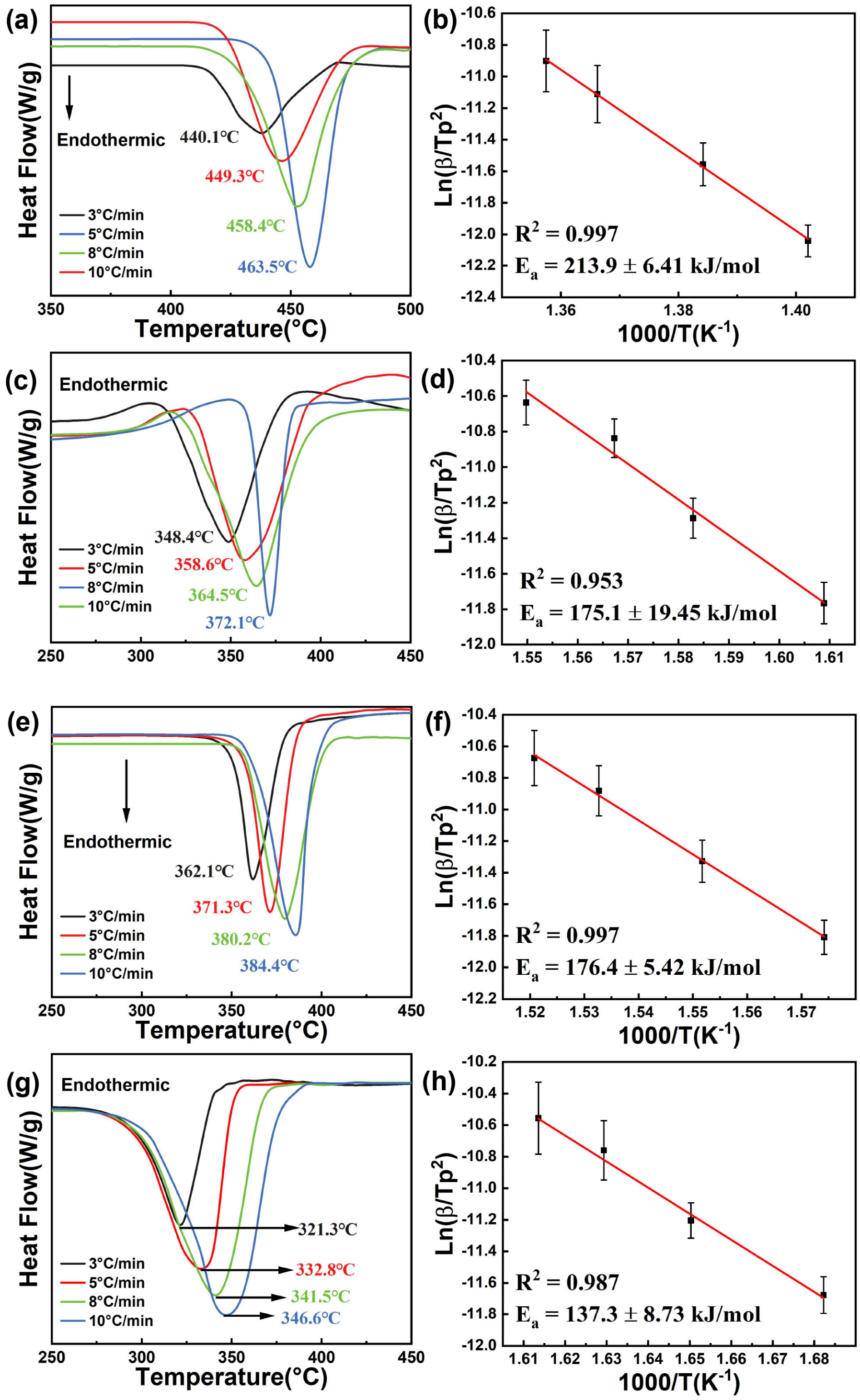

Figure 5. DSC curves and Arrhenius equation of (**a**,**b**) pure MgH_2, (**c**,**d**) MgH_2@CC, (**e**,**f**) BM-MgH_2 and (**g**,**h**) MgH_2-CC.

2.2.2. Thermodynamic Properties of MgH_2@CC and MgH_2-CC Composites

Thermodynamic tests were based on the equilibrium pressure of the desorption platform in PCI at different temperatures. The enthalpy (ΔH) and entropy (ΔS) of deuterium desorption were determined according to the van't Hoff equation:

$$\ln\left(\frac{P_e}{P_0}\right) = \left(\frac{\Delta H}{RT}\right) - \left(\frac{\Delta S}{R}\right) \tag{3}$$

where P_e is the equilibrium desorption pressure, P_0 is the standard atmospheric pressure, R is the gas constant, and T is the temperature in Kelvin.

To investigate the thermodynamic properties of MgH_2@CC and MgH_2-CC composites, as shown in Figure 6a–d, P-C-T tests were performed at 275 °C, 300 °C, 325 °C, and 350 °C, and the hydrogen absorption and release plateau pressures were obtained for the corresponding temperatures. The plateau pressures (P_{eq}) at different temperatures are shown in Table 1, and each plateau pressure is positively correlated with the temperature; ΔH and ΔS were calculated according to the Van't Hoff Equation (3). Based on the slope and intercept of the straight line in the fitting results, the enthalpy changes of hydrogen release (ΔH_{des}) and entropy change of hydrogen release (ΔS_{des}) of MgH_2@CC composites are 73.5 $kJ \cdot mol^{-1}$ and 140.5 $J \cdot mol^{-1} \cdot K^{-1}$, respectively, and the enthalpy change of hydrogen absorption (ΔH_{abs}) and entropy change of hydrogen absorption (ΔS_{abs}) were −71.7 $kJ \cdot mol^{-1}$ and −132.2 $J \cdot mol^{-1} \cdot K^{-1}$, respectively. The enthalpy changes of hydrogen release ΔH_{des} and entropy change of hydrogen release ΔS_{des} of MgH_2-CC composites were 73.0 $kJ \cdot mol^{-1}$ and 140.5 $J \cdot mol^{-1} \cdot K^{-1}$, respectively, and the enthalpy change of hydrogen absorption ΔH_{abs} and entropy change of hydrogen absorption ΔS_{abs} were −72.8 $kJ \cdot mol^{-1}$ and −136.2 $J \cdot mol^{-1} \cdot K^{-1}$, respectively. Compared with the commercially pure MgH_2 (ΔH_{des} = 76 kJ/mol^{-1} and ΔS_{des} = 134.1 $J \cdot mol^{-1} \cdot K^{-1}$), the thermodynamic properties have not been improved, indicating that reducing the size of the MgH_2 particle size and preventing MgH_2 particle aggregation is more likely to be reflected in the improvement of kinetic properties.

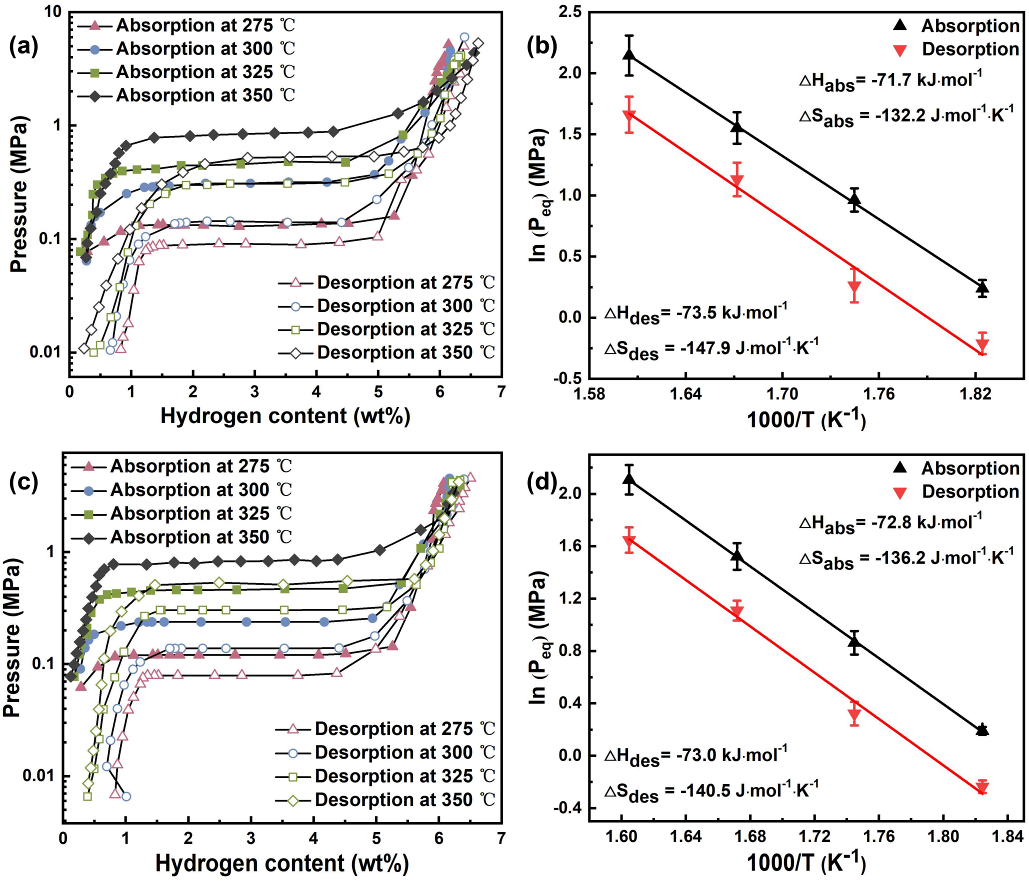

Figure 6. P-C-T curves and Van't Hoff equation of (**a**,**b**) MgH_2@CC composites and (**c**,**d**) MgH_2-CC composites.

Table 1. Hydrogen absorption and desorption plateau of MgH_2@CC and MgH_2-CC composite under different temperature.

Temperature (°C)	Absorption Plateau (MPa)		Desorption Plateau (MPa)	
	MgH_2@CC	MgH_2-CC	MgH_2@CC	MgH_2-CC
350	0.853	0.823	0.526	
325	0.472	0.458	0.310	0.303
300	0.262	0.237	0.130	0.138
275	0.127	0.121	0.081	0.079

2.3. Mechanism Understanding

In order to investigate the reason for the enhanced hydrogen release properties of MgH_2@CC composites, Fourier Transform Infrared Spectroscopy (FTIR) was conducted to analyze the material; the results are shown in Figure 7a. Among them, the peaks in the 1150–1500 cm^{-1} region correspond to the Mg-H stretching bands, the peaks in the 759–1000 cm^{-1} region correspond to the Mg-H bending bands, and the peaks in the 1450–1550 cm^{-1} region correspond to the O-H bonding, which means that the material undergoes partial oxidation. The peaks in the 2850–2960 cm^{-1} region correspond to the C-H bonding, which means that the carbon fiber matrix interacts with MgH_2 at the hydrogen release stage; this implies that the carbon fiber matrix interacts with MgH_2 during the hydrogen release phase [51–53]. When the hydrogen absorption reaction occurs, the carbon in magnesium-carbon composites adsorbs hydrogen from H_2 atmosphere or MgH_2 to form sp^2 C-H and sp^3 C-H bands [54]. When the hydrogen release reaction occurs, the carbon becomes a carrier for H atom transfer due to the C-H bond [55,56], the high temperature energy will drive the C-H bond to break, and the broken carbon bond will act as a carrier for H transfer and reduce the activation energy of the Mg-H bond, which will promote MgH_2 to overcome the hydrogen release energy barrier, similar to the photocatalytic Ni/TiO_2 composites, where the electrons are excited by the visible light and transferred from Ni to Ti, which drives the photocatalytic hydrogen production [57]. The activation energy is reduced, which improves the hydrogen storage performance of MgH_2@CC composites. In contrast, in MgH_2-CC composites, Mg has more binding sites with C. The C-H bonds and high-energy ball mills synergize with each other to provide more reaction sites and energy for hydrogen uptake/desorption, and thus produce better catalytic effects. The schematic diagram of the desorption enhancement mechanism of magnesium-carbon composites is shown in Figure 7b.

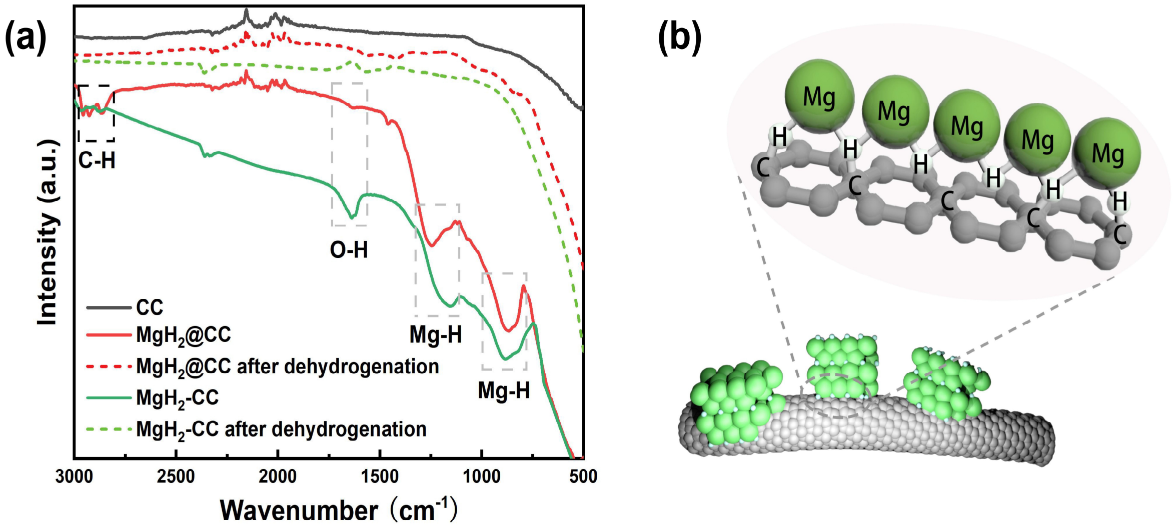

Figure 7. (**a**) FTIR images of MgH_2@CC composite and MgH_2-CC composites and (**b**) Schematic diagram of the enhanced mechanism for desorption of magnesium-carbon composites.

3. Experimental

3.1. Material Preparation

Carbon fiber cloth (CDD, 200 × 200 mm, Yongfu Electrochemical, Nanajing, China) was purchased and further processed. Dibutyl magnesium (1.0 mol/L in heptane, Aladdin, solution), MgH_2 (>95% from Mg Power Technology Co., Ltd., Shanghai, China), and anhydrous ethanol (C_2H_5OH, AR, Anhui Tiandi High Purity, Anqing, Anhui) were purchased and directly used as received without further purification. First, as shown in Figure 1a, the carbon fiber cloth was pretreated. The carbon fiber cloth was rinsed with ethanol, dried in an oven, and then placed in a stainless-steel autoclave and heated at 300 °C under 2 MPa hydrogen atmosphere for 3 h to remove hydrophilic groups and other impurities. In a sealed glove box filled with argon gas, weigh 0.43 g of pretreated carbon fiber cloth into a beaker and draw up a total of 3 mL of dibutyl magnesium solution using a syringe with a volume capacity of 5 mL. The absorbed solution was added to the surface of the carbon fiber cloth with 0.5 mL drops at a time, and after the carbon fiber cloth was completely impregnated, another drop was added until 3 mL was added. Subsequently, the beaker was placed in a vacuum chamber and vacuum dried for 12 h to remove the heptane solvent to obtain $MgBu_2$@CC. Finally, the sample was placed in a stainless-steel sample chamber and kept at 5 MPa hydrogen pressure and 200 °C for 2 h. The final sample obtained was named as MgH_2@CC composite. Subsequently, the sample was vacuum-dried in a vacuum oven at 80 °C for 6 h to obtain the carbon fiber-loaded precursor composite. The equation of the reaction was as follows:

$$(C_4H_9)_2Mg + 2H_2 \rightarrow MgH_2 + 2C_4H_9 \quad (4)$$

The loading of MgH_2 in MgH_2@CC can be calculated to be ~24.2 wt% from the before and after mass difference.

MgH_2-CC composites were prepared as shown in Figure 1b. In an argon glove box, pure MgH_2 and carbon fiber cloth were weighed according to the mass percentage of 75:25 and put into a stainless-steel ball milling jar with a ball to material ratio of 40:1. The stainless-steel balls were DECO-304-B, with diameters of 5 mm, 6 mm, 8 mm, and 10 mm, respectively. The ball milling time was 10 h. The ball milling speed was 400 rpm, and the interval between each 30-min revolution of the ball mill was 5 min. Ball milled MgH_2 (BM-MgH_2) samples were prepared in the same way described above.

3.2. Material Characterization

The phase composition of the composites was analysed by using an X-ray diffractometer (XRD, Mini Flex 600, Rigaku, Japan) with Cu Kα radiation (λ = 0.154056 nm) at 40 kV and 15 mA. The 2θ angle ranged from 10° to 90°with increments of 0.02°; samples were placed in a hermetically sealed XRD sample stage and sealed with polymer tape. The morphologies and microstructures of the samples were examined by using scanning electron microscopy (SEM, MIRA3 XMU, Tescan). We analysed the elemental distribution in the local region of the samples by EDS (Xplore30, OXFORD) attached to SEM, with magnification rates ranging from 200 to 5000. For SEM samples, ethanol or organic magnesium was used as the dispersant, and a small amount of the solution was taken and dropped on the conductive adhesive after sonication. SEM tests were performed at magnifications of 5 K, 10 K, and 20 K, with a 5 kv energy. Thermogravimetric analysis (TG, DTG-60H, SHIMADZU) was performed in the range of 30~700 °C with a heating rate of 10 °C/min to verify the loaded composition, Weigh about 5 mg of the sample in the glove box, place it in an aluminium crucible with a lid to seal the aluminium crucible and then take it out and put it into the DTG-60H instrument for testing. Maintain the argon gas environment at 0.2 Mpa during the testing process with a flow rate of 300 mL/min, and determine the peak value by selecting the beginning and end intervals of the melting peak in the DSC test. Raman spectra (HORIBA LabRAM HR Evolution spectrometer) were measured and processed with a laser wavelength of 532 nm. Fourier Transform Infrared Spectroscopy (FTIR) was conducted to analyse the material with a detection wavelength range of 500~3000 cm^{-1}. The samples were mixed with KBr and then pelletized in the argon-filled glove box.

The thermodynamic properties were evaluated by measuring the pressure−composition isotherms (PCI) on an automatic Sievert-type apparatus. Prior to the PCI measurements, we weighed 0.1–0.5 g of sample and heated it at 300 °C under vacuum conditions and activated it through two hydrogen sorption cycles consisting of a 0.5 h absorption under 3.0 MPa of H_2 gas and a 0.5 h desorption under vacuum. All the tests were performed under initial pressures of 0.0001 MPa for desorption and 5 MPa hydrogen pressure for absorption.

4. Conclusions

In summary, two carbon fiber-loaded MgH_2 hydrogen storage composites were successfully prepared by hydrogenation of organic magnesium and ball milling. Both the obtained MgH_2@CC and MgH_2-CC composites show significantly improved kinetics, with the MgH_2-CC composite being better in terms of preparation cost and kinetics. Our experimental results reveal that C-H bonding interactions in the two composite hydrogen storage materials are responsible for promoted hydrogen absorption/desorption from hydrides. These results provide further insights into promoting the hydrogen ab-/desorption of metal hydrides. Unfortunately, the thermodynamics were not improved, and we will work on the improvement of thermodynamic properties in subsequent work.

Author Contributions: Conceptualization, Q.Y. and X.D.; Methodology, X.J.; Validation, Z.Q.; Formal analysis, Q.Y.; Investigation, X.J.; Writing—original draft, Q.Y.; Writing—review & editing, X.D.; Visualization, Z.Q.; Supervision, Y.L.; Project administration, Y.L. All authors have read and agreed to the published version of the manuscript.

Funding: This work was financially supported by the National Natural Science Foundation of China (No. 52471027), the Natural Science Foundation of Anhui Province (No. 2308085QB50), the Natural Science Foundation of Anhui Provincial Education Department (Nos. KJ2021A0393, 2022AH020033 and 2022AH010025).

Data Availability Statement: Data is contained within the article.

Conflicts of Interest: The authors declare no conflicts of interest.

References

1. Zhang, J.; Li, Z.; Wu, Y.; Guo, X.; Ye, J.; Yuan, B.; Wang, S.; Jiang, L. Recent Advances on the Thermal Destabilization of Mg-Based Hydrogen Storage Materials. *RSC Adv.* **2019**, *9*, 408–428. [CrossRef] [PubMed]
2. Bolarin, J.A.; Zou, R.; Li, Z.; Munyentwali, A.; Zhang, Z.; Cao, H. Recent Path to Ultrafine Mg/MgH_2 Synthesis for Sustainable Hydrogen Storage. *Int. J. Hydrogen Energy* **2024**, *52*, 251–274. [CrossRef]
3. Yang, F.; Wang, J.; Zhang, Y.; Wu, Z.; Zhang, Z.; Zhao, F.; Huot, J.; Grobivć Novaković, J.; Novaković, N. Recent Progress on the Development of High Entropy Alloys (HEAs) for Solid Hydrogen Storage: A Review. *Int. J. Hydrogen Energy* **2022**, *47*, 11236–11249. [CrossRef]
4. Baum, Z.J.; Diaz, L.L.; Konovalova, T.; Zhou, Q.A. Materials Research Directions Toward a Green Hydrogen Economy: A Review. *ACS Omega* **2022**, *7*, 32908–32935. [CrossRef]
5. Lu, Y.; Kim, H.; Sakaki, K.; Hayashi, S.; Jimura, K.; Asano, K. Destabilizing the Dehydrogenation Thermodynamics of Magnesium Hydride by Utilizing the Immiscibility of Mn with Mg. *Inorg. Chem.* **2019**, *58*, 14600–14607. [CrossRef]
6. Qin, Z.-K.; He, L.-Q.; Ding, X.-L.; Si, T.-Z.; Cui, P.; Li, H.-W.; Li, Y.-T. Liquid Channels Built-In Solid Magnesium Hydrides for Boosting Hydrogen Sorption. *Inorganics* **2023**, *11*, 216. [CrossRef]
7. Chen, Y.; Habibullah; Xia, G.; Jin, C.; Wang, Y.; Yan, Y.; Chen, Y.; Gong, X.; Lai, Y.; Wu, C. Hydrogen Storage Properties of Economical Graphene Materials Modified by Non-Precious Metal Nickel and Low-Content Palladium. *Inorganics* **2023**, *11*, 251. [CrossRef]
8. Xu, Y.; Zhou, Y.; Li, Y.; Ding, Z. Carbon-Based Materials for Mg-Based Solid-State Hydrogen Storage Strategies. *Int. J. Hydrogen Energy* **2024**, *69*, 645–659. [CrossRef]
9. Floriano, R.; Zepon, G.; Edalati, K.; Fontana, G.L.B.G.; Mohammadi, A.; Ma, Z.; Li, H.-W.; Contieri, R.J. Hydrogen Storage in TiZrNbFeNi High Entropy Alloys, Designed by Thermodynamic Calculations. *Int. J. Hydrogen Energy* **2020**, *45*, 33759–33770. [CrossRef]
10. Mohammadi, A.; Ikeda, Y.; Edalati, P.; Mito, M.; Grabowski, B.; Li, H.-W.; Edalati, K. High-Entropy Hydrides for Fast and Reversible Hydrogen Storage at Room Temperature: Binding-Energy Engineering via First-Principles Calculations and Experiments. *Acta Mater.* **2022**, *236*, 118117. [CrossRef]

11. Cao, W.; Ding, X.; Chen, R.; Zhang, J.; Zhang, Y.; Guo, J.; Fu, H. Dual Tuning of the De-/Hydrogenation Thermodynamics and Kinetics of the Mg–Ni Alloy by Introducing the Ag–H Bond: Enhanced Hydrogen Storage Properties at Moderate Temperatures. *J. Mater. Chem. A* **2023**, *11*, 20761–20773. [CrossRef]
12. Panigrahi, P.K.; Chandu, B.; Motapothula, M.R.; Puvvada, N. Potential Benefits, Challenges and Perspectives of Various Methods and Materials Used for Hydrogen Storage. *Energy Fuels* **2024**, *38*, 2630–2653. [CrossRef]
13. Zhou, C.; Zhang, J.; Bowman, R.C.; Fang, Z.Z. Roles of Ti-Based Catalysts on Magnesium Hydride and Its Hydrogen Storage Properties. *Inorganics* **2021**, *9*, 36. [CrossRef]
14. Zhou, C.; Fang, Z.Z.; Lu, J.; Zhang, X. Thermodynamic and Kinetic Destabilization of Magnesium Hydride Using Mg–In Solid Solution Alloys. *J. Am. Chem. Soc.* **2013**, *135*, 10982–10985. [CrossRef] [PubMed]
15. Kefi, C.; Huot, J. Entropy-Enthalpy Compensation in Ti-V-Mn-Cr BCC Alloys Used as Hydrogen Storage Materials. *Inorganics* **2023**, *11*, 479. [CrossRef]
16. Zhang, Q.; Fang, M.; Si, T.; Fang, F.; Sun, D.; Ouyang, L.; Zhu, M. Phase Stability, Structural Transition, and Hydrogen Absorption−Desorption Features of the Polymorphic La_4MgNi_{19} Compound. *J. Phys. Chem. C* **2010**, *114*, 11686–11692. [CrossRef]
17. Zhou, C.; Peng, Y.; Zhang, Q. Growth Kinetics of MgH_2 Nanocrystallites Prepared by Ball Milling. *J. Mater. Sci. Technol.* **2020**, *50*, 178–183. [CrossRef]
18. Zhang, Q.A.; Liu, D.D.; Wang, Q.Q.; Fang, F.; Sun, D.L.; Ouyang, L.Z.; Zhu, M. Superior Hydrogen Storage Kinetics of $Mg_{12}YNi$ Alloy with a Long-Period Stacking Ordered Phase. *Scr. Mater.* **2011**, *65*, 233–236. [CrossRef]
19. Ding, X.; Li, Y.; Fang, F.; Sun, D.; Zhang, Q. Hydrogen-Induced Magnesium–Zirconium Interfacial Coupling: Enabling Fast Hydrogen Sorption at Lower Temperatures. *J. Mater. Chem. A* **2017**, *5*, 5067–5076. [CrossRef]
20. Zhang, K.; Chang, Y.; Lei, J.; Chen, J.; Si, T.; Ding, X.; Cui, P.; Li, H.-W.; Zhang, Q.; Li, Y. Synergy of inside Doped metals–Outside Coated Graphene to Enhance Hydrogen Storage in Magnesium-Based Alloys. *J. Magnes. Alloys* **2024**, *12*, 2462–2471. [CrossRef]
21. Aguey-Zinsou, K.-F.; Ares-Fernández, J.-R. Hydrogen in Magnesium: New Perspectives toward Functional Stores. *Energy Environ. Sci.* **2010**, *3*, 526. [CrossRef]
22. Lotoskyy, M.; Denys, R.; Yartys, V.A.; Eriksen, J.; Goh, J.; Nyamsi, S.N.; Sita, C.; Cummings, F. An Outstanding Effect of Graphite in Nano-MgH_2–TiH_2 on Hydrogen Storage Performance. *J. Mater. Chem. A* **2018**, *6*, 10740–10754. [CrossRef]
23. Yan, S.; Wei, L.; Gong, Y.; Yang, K. Enhanced Hydrogen Storage Properties of Magnesium Hydride by Multifunctional Carbon-Based Materials: A Review. *Int. J. Hydrogen Energy* **2024**, *55*, 521–541. [CrossRef]
24. Zhang, X.L.; Liu, Y.F.; Zhang, X.; Hu, J.J.; Gao, M.X.; Pan, H.G. Empowering Hydrogen Storage Performance of MgH_2 by Nanoengineering and Nanocatalysis. *Mater. Today Nano* **2020**, *9*, 100064. [CrossRef]
25. Zhang, X.; Liu, Y.; Ren, Z.; Zhang, X.; Hu, J.; Huang, Z.; Lu, Y.; Gao, M.; Pan, H. Realizing 6.7 Wt% Reversible Storage of Hydrogen at Ambient Temperature with Non-Confined Ultrafine Magnesium Hydrides. *Energy Environ. Sci.* **2021**, *14*, 2302–2313. [CrossRef]
26. Liu, M.; Zhao, S.; Xiao, X.; Chen, M.; Sun, C.; Yao, Z.; Hu, Z.; Chen, L. Novel 1D Carbon Nanotubes Uniformly Wrapped Nanoscale MgH_2 for Efficient Hydrogen Storage Cycling Performances with Extreme High Gravimetric and Volumetric Capacities. *Nano Energy* **2019**, *61*, 540–549. [CrossRef]
27. El-Eskandarany, M.S.; Ali, N.; Al-Ajmi, F.; Banyan, M.; Al-Duweesh, A.A. Hydrogen Storage Behavior and Performance of Multiple Cold-Rolled MgH_2/Nb_2O_5 Nanocomposite Powders. *Processes* **2022**, *10*, 1017. [CrossRef]
28. Maafa, I.M.; Zouli, N.; Abutaleb, A.; Yousef, A.; Qudsieh, I.Y.; Matar, S.M.; Adam, A.S.M.; El-Halwany, M.M. In Situ Preparation of 2D Co-B Nanosheets@1D TiO_2 Nanofibers as a Catalyst for Hydrogen Production from Sodium Borohydride. *Inorganics* **2023**, *11*, 342. [CrossRef]
29. Mehrabi, M.; Reyhani, A.; Parvin, P.; Mortazavi, S.Z. Surface Structural Alteration of Multi-Walled Carbon Nanotubes Decorated by Nickel Nanoparticles Based on Laser Ablation/Chemical Reduction Methods to Enhance Hydrogen Storage Properties. *Int. J. Hydrogen Energy* **2019**, *44*, 3812–3823. [CrossRef]
30. Mehrabi, M.; Parvin, P.; Reyhani, A.; Mortazavi, S.Z. Hybrid Laser Ablation and Chemical Reduction to Synthesize Ni/Pd Nanoparticles Decorated Multi-Wall Carbon Nanotubes for Effective Enhancement of Hydrogen Storage. *Int. J. Hydrogen Energy* **2018**, *43*, 12211–12221. [CrossRef]
31. Li, Z.-Y.; Sun, L.-X.; Xu, F.; Luo, Y.-M.; Xia, Y.-P.; Wei, S.; Zhang, C.-C.; Cheng, R.-G.; Ye, C.-F.; Liu, M.-Y.; et al. Modulated Noble Metal/2D MOF Heterostructures for Improved Hydrogen Storage of MgH_2. *Rare Met.* **2024**, *43*, 1672–1685. [CrossRef]
32. Zhang, Q.; Huang, Y.; Ma, T.; Li, K.; Ye, F.; Wang, X.; Jiao, L.; Yuan, H.; Wang, Y. Facile Synthesis of Small MgH_2 Nanoparticles Confined in Different Carbon Materials for Hydrogen Storage. *J. Alloys Compd.* **2020**, *825*, 153953. [CrossRef]
33. Liu, Y.; Zou, J.; Zeng, X.; Wu, X.; Tian, H.; Ding, W.; Wang, J.; Walter, A. Study on Hydrogen Storage Properties of Mg Nanoparticles Confined in Carbon Aerogels. *Int. J. Hydrogen Energy* **2013**, *38*, 5302–5308. [CrossRef]
34. Satawara, A.M.; Shaikh, G.A.; Gupta, S.K.; Andriotis, A.N.; Menon, M.; Gajjar, P.N. An Ab-Initio Analysis of the Hydrogen Storage Behaviour of V Doped Si_2BN Nanotube. *Int. J. Hydrogen Energy* **2024**, *52*, 1560–1567. [CrossRef]
35. Abutaleb, A. Synthesis of Copper/Sulfur Co-Doped TiO_2-Carbon Nanofibers as Catalysts for H_2 Production via $NaBH_4$ Hydrolysis. *Inorganics* **2023**, *11*, 352. [CrossRef]
36. Zeng, L.; Qing, P.; Cai, F.; Huang, X.; Liu, H.; Lan, Z.; Guo, J. Enhanced Hydrogen Storage Properties of MgH_2 Using a Ni and TiO_2 Co-Doped Reduced Graphene Oxide Nanocomposite as a Catalyst. *Front. Chem.* **2020**, *8*, 207. [CrossRef]
37. Boateng, E.; Thiruppathi, A.R.; Hung, C.-K.; Chow, D.; Sridhar, D.; Chen, A. Functionalization of Graphene-Based Nanomaterials for Energy and Hydrogen Storage. *Electrochim. Acta* **2023**, *452*, 142340. [CrossRef]

38. Mahamiya, V.; Shukla, A.; Chakraborty, B. Scandium Decorated C24 Fullerene as High Capacity Reversible Hydrogen Storage Material: Insights from Density Functional Theory Simulations. *Appl. Surf. Sci.* **2022**, *573*, 151389. [CrossRef]
39. EL-Barbary, A.A.; Shabi, A.H. Stone-Wales Defective C60 Fullerene for Hydrogen Storage. *Int. J. Hydrogen Energy* **2024**, *71*, 155–164. [CrossRef]
40. Kumar, P.; Singh, S.; Hashmi, S.A.R.; Kim, K.-H. MXenes: Emerging 2D Materials for Hydrogen Storage. *Nano Energy* **2021**, *85*, 105989. [CrossRef]
41. Huang, T.; Huang, X.; Hu, C.; Wang, J.; Liu, H.; Xu, H.; Sun, F.; Ma, Z.; Zou, J.; Ding, W. MOF-Derived Ni Nanoparticles Dispersed on Monolayer MXene as Catalyst for Improved Hydrogen Storage Kinetics of MgH_2. *Chem. Eng. J.* **2021**, *421*, 127851. [CrossRef]
42. Su, Y.; Yang, M.; Wang, X.; Tian, F.; Jia, H.; Li, L. Synthesis of Ni Nanoparticles Embedded Porous Mo_2C Nanospheres for Enhancing the Electrochemical Hydrogen Storage Properties of Co_2B Material. *J. Alloys Compd.* **2023**, *954*, 170143. [CrossRef]
43. Tseng, F.-G.; Bhalothia, D.; Lo, K.-H.; Syu, C.-H.; Chen, Y.-C.; Sihag, A.; Wang, C.-W.; Chen, H.-Y.T.; Chen, T.-Y. Glucose-Based Highly-Porous Activated Carbon Nanospheres (g-ACNSs) for High Capacity Hydrogen Storage. *Energy Adv.* **2024**, *3*, 1283–1292. [CrossRef]
44. Alsabawi, K.; Webb, T.A.; Gray, E.; Webb, C.J. The Effect of C60 Additive on Magnesium Hydride for Hydrogen Storage. *Int. J. Hydrogen Energy* **2015**, *40*, 10508–10515. [CrossRef]
45. Lakhnik, A.; Kirian, I.; Rud, A. Comparative Analysis of Hydrogen Uptake and Release Kinetics in MgH_2/C Composites Synthesized Using Varied Surface Areas Graphite Powders. *Appl. Phys. A* **2024**, *130*, 283. [CrossRef]
46. Guo, S.; Yu, Z.; Li, Y.; Fu, Y.; Zhang, Z.; Han, S. Preparation of Mg-Mg_2Ni/C Composite and Its Excellent Hydrogen Storage Properties. *J. Alloys Compd.* **2024**, *976*, 173035. [CrossRef]
47. Carson, R.M.; Ellis, B.L.; Long, F.; Persaud, S.Y. Structural Evolution of a Mg–C Composite over 1000 H_2 Storage Cycles. *Int. J. Hydrogen Energy* **2024**, *51*, 676–687. [CrossRef]
48. Huang, Y.; Li, M.; Liang, T.; Zhou, Y.; Guan, P.; Zhou, L.; Hu, L.; Wan, T.; Chu, D. Structural Optimization and Electrocatalytic Hydrogen Production Performance of Carbon-Based Composites: A Mini-Review. *Carbon Trends* **2024**, *15*, 100363. [CrossRef]
49. Qiao, Z.; Bian, K.; Ding, C.; Zhao, Y. Recent Progress of Carbon-Fiber-Based Electrode Materials for Energy Storage. *Diam. Relat. Mater.* **2023**, *138*, 110208. [CrossRef]
50. Fang, B.; Li, L.; Guo, J.; Qin, Y.; Wei, Y.; Zhang, J.; He, C.; Chen, Y. Development of a Novel Co-Doped Carbon Fiber from Textile Waste as Catalyst for the Highly Efficient Degradation of Organic Pollutants: The Key Role of C–O–Co Bond. *Chem. Eng. J.* **2024**, *498*, 155494. [CrossRef]
51. Mishra, M.K.; Ghalsasi, P.; Deo, M.N.; Bhatt, H.; Poswal, H.K.; Ghosh, S.; Ganguly, S. In Situ High Pressure Study of an Elastic Crystal by FTIR Spectroscopy. *CrystEngComm* **2017**, *19*, 7083–7087. [CrossRef]
52. Amaral, M.M.; Yukuhiro, V.Y.; Vicentini, R.; Peterlevitz, A.C.; Da Silva, L.M.; Fernandez, P.; Zanin, H. Direct Observation of the CO_2 Formation and C–H Consumption of Carbon Electrode in an Aqueous Neutral Electrolyte Supercapacitor by in-Situ FTIR and Raman. *J. Energy Chem.* **2022**, *71*, 488–496. [CrossRef]
53. Song, Y.; Zhang, T.; Zhou, S.; Liu, P.; Yu, H.; Han, Z. Confinement of Mg Nanoparticles by Bituminous Coal and Associated Synergistic Hydrogen Storage Effect. *J. Mater. Eng Perform* **2020**, *29*, 760–768. [CrossRef]
54. Peng, C.; Li, Y.; Zhang, Q. Enhanced Hydrogen Desorption Properties of MgH_2 by Highly Dispersed Ni: The Role of in-Situ Hydrogenolysis of Nickelocene in Ball Milling Process. *J. Alloys Compd.* **2022**, *900*, 163547. [CrossRef]
55. Salamone, M.; Martin, T.; Milan, M.; Costas, M.; Bietti, M. Electronic and Torsional Effects on Hydrogen Atom Transfer from Aliphatic C–H Bonds: A Kinetic Evaluation via Reaction with the Cumyloxyl Radical. *J. Org. Chem.* **2017**, *82*, 13542–13549. [CrossRef]
56. Capaldo, L.; Ravelli, D.; Fagnoni, M. Direct Photocatalyzed Hydrogen Atom Transfer (HAT) for Aliphatic C–H Bonds Elaboration. *Chem. Rev.* **2022**, *122*, 1875–1924. [CrossRef]
57. Fan, L.; Long, J.; Gu, Q.; Huang, H.; Lin, H.; Wang, X. Single-Site Nickel-Grafted Anatase TiO_2 for Hydrogen Production: Toward Understanding the Nature of Visible-Light Photocatalysis. *J. Catal.* **2014**, *320*, 147–159. [CrossRef]